NANO LETTERS

pubs.acs.org/NanoLett

Immobilization of Gold Nanoparticles on Living Cell Membranes upon Controlled Lipid Binding

Haojin Ba, Jessica Rodríguez-Fernández,* Fernando D. Stefani,† and Jochen Feldmann

Photonics and Optoelectronics Group and CeNS, Physics Department, Ludwig-Maximilians-Universität München, Amalienstr. 54, 80799 Munich, Germany

ABSTRACT We present a versatile and controlled route to immobilize gold nanoparticles (NPs) on the surface of living cells, while preserving the sensing and optothermal capabilities of the original colloid. Our approach is based on the controlled and selective binding of Au NPs to phospholipids prior to cell incubation. We show that in the presence of the cells the lipid-bound Au NPs are delivered to the cellular membrane and that their diffusion is rather slow and spatially limited, as a result of lipid binding. Avoiding nonspecific membrane labeling, this approach is of general application to several types of colloids and cells and thereby provides a platform for controlled plasmonic and optothermal investigations of living cell membranes.

KEYWORDS Gold nanoparticles, surface modification, lipid binding, cell membrane, labeling, diffusion

A large number of vital processes, such as photosynthesis, nutrient recognition, and signaling, occur across or at the membranes of biological cells.[1] Mapping, sensing, and manipulation of cellular membranes and their related processes have focused a great deal of attention, and the applicability of several nanomaterials, such as quantum dots,[2,3] magnetic nanoparticles,[4] or carbon nanotubes,[5] is being actively explored. Gold nanoparticles have emerged as appealing optical markers for living cells due to their chemical stability and unique optical properties.[6] Sensing cell membrane processes with gold colloids may benefit not only from the high sensitivity of their localized surface plasmon resonance[7,8] but also from their potential as ultrasensitive surface enhanced Raman scattering (SERS) reporters.[9] Moreover, the spatially confined thermal manipulation of the plasma membrane can become feasible by irradiating the gold cores with an external laser source.[10,11] Undoubtedly, the controlled labeling of living plasma membranes with Au nanoparticles opens up a powerful optical toolbox for the investigation and manipulation of cell membrane processes.

To date, a number of approaches have been exploited for cell surface labeling with Au colloids. Several methods rely on the unspecific and rather uncontrolled electrostatic attachment of weakly stabilized nanoparticles to the cellular surface,[12,13] which usually results on particle aggregation under physiological conditions. Others deal with the direct adsorption or surface functionalization of the nanoparticles with ligands/antibodies that specifically bind to membrane receptors/antigens.[14,15] The latter approaches are useful for membrane protein studies but do not provide the freedom for general cell membrane investigations and may be disadvantageous for some applications. For example, plasmonic heating investigations may be limited because thermal changes can easily induce protein denaturation and subsequent loss of biological function. Furthermore, the plasmon sensing capability can be reduced as a result of the large coating thickness imposed by the size of the proteins. Clearly, in order to exploit the full capabilities of Au nanoparticles as active nanotools on cellular membranes, ways to attach them controllably and directly to membrane lipids are needed.

Here, we present a general, versatile, and controlled strategy to immobilize gold nanoparticles on cellular membranes, while retaining their full capabilities for sensing and optothermal manipulation in living cells. Our approach is based on Au nanoparticle (NP)/lipid binding prior to cell incubation and therefore avoids the nonspecific, uncontrolled anchoring of the NPs to random cell membrane components. CTAB (cetyltrimethylammonium bromide) is a surfactant extensively used in the synthesis of noble metal, as well as magnetic, nanoparticles of varying sizes and shapes.[16−20] Hence, for the general applicability of our labeling approach we have selected CTAB-stabilized Au nanospheres as a model colloid. We first modify the surface chemistry of CTAB-capped gold nanospheres. Our surface modification strategy involves poly(ethylene glycol) (PEG) grafting and maleimide derivatization. Second, the nanoparticles are chemically anchored to phospholipids in liposomes via maleimide−thiol reactivity. Finally, liposome−cell membrane fusogenesis enables the delivery of the lipid-

* To whom correspondence should be addressed, jesica.rodriguez@physik.uni-muenchen.de.

† Current address: Departamento de Física & Instituto de Física de Buenos Aires (IFIBA, CONICET), Facultad de Ciencias Exactas y Naturales, Universidad de Buenos Aires, Pabellón I Ciudad Universitaria, 1428 Buenos Aires, Argentina.

Received for review: 04/25/2010
Published on Web: 07/08/2010

DOI: 10.1021/nl101454a | *Nano Lett.* **2010,** *10,* 3006–3012

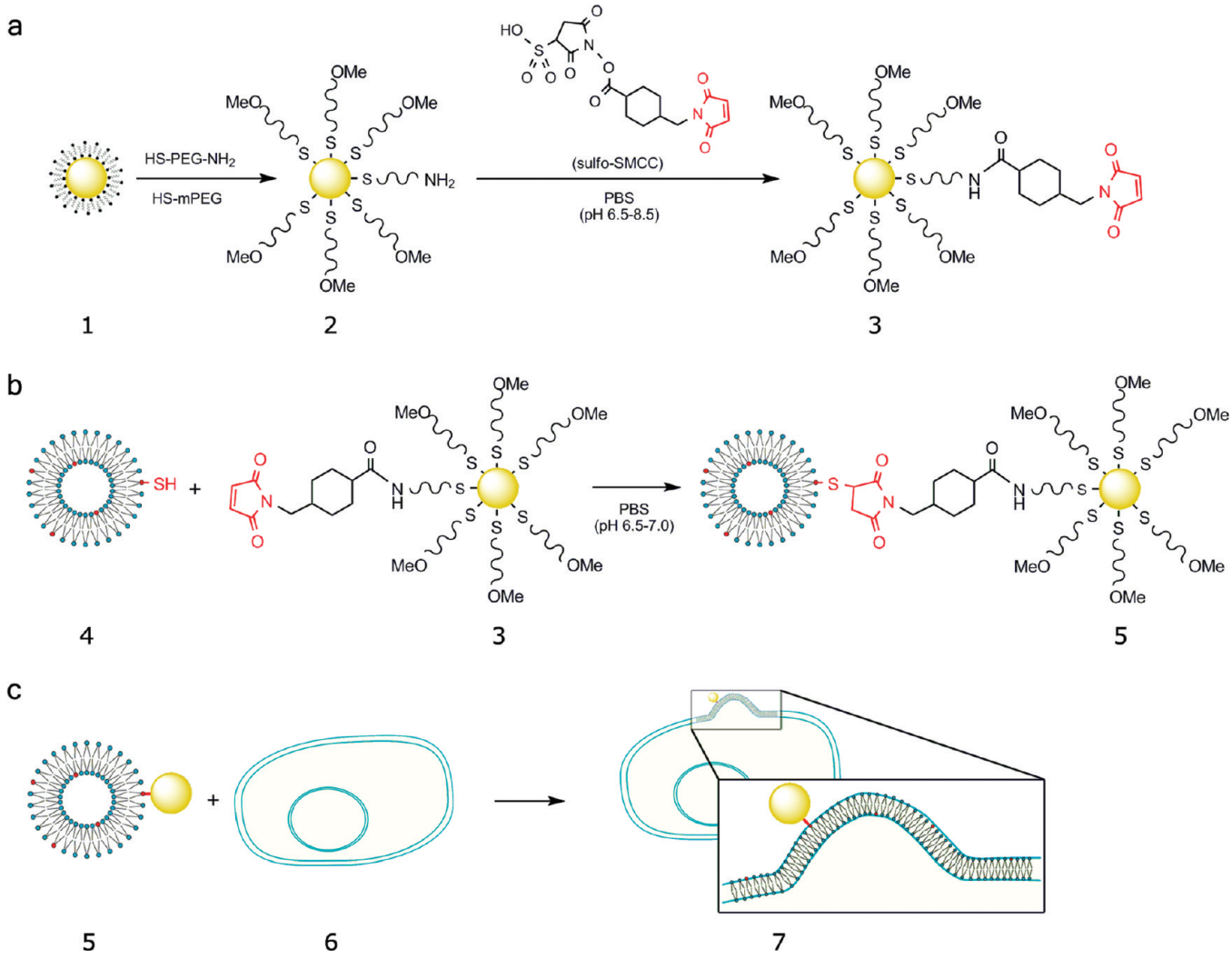

FIGURE 1. Sketch depicting the general strategy for surface modification, lipid binding, and final cell membrane incorporation of Au nanoparticles. (a) PEGylation and subsequent maleimide functionalization of CTAB-capped Au nanospheres. (b) Conjugation of the maleimide-functionalized nanoparticles to liposomes containing a thiolated lipid (PTE−SH). (c) Fusion of the Au@mal-tagged liposomes with the cell membrane of Jurkat cells. The numbers refer to Au@CTAB (1), Au@mPEG−SH/HS−PEG−NH_2 (2), and Au@mal (3) nanoparticles, respectively; small liposomes containing PTE−SH (4), Au@mal bound to PTE−SH in liposomes (5), living (Jurkat) cell (6), and Au@mal tagged to PTE−SH in the cell membrane, after liposome/membrane fusogenesis (7).

bound Au NPs to the cellular surface. We show that as a result of lipid tagging the diffusion of the Au NPs on the cell membrane is limited. Our strategy may be generally applied to incorporate CTAB-capped nanoparticles of varying composition, size, or morphology on the membrane of different cells, enabling the realization of controlled mapping, probing, and manipulation experiments.

Figure 1 schematically depicts the general strategy that we have used. The first step (Figure 1a) consists of the exchange of CTAB molecules from the Au nanoparticle surface (Au@CTAB, **1**) with a mixture of mono-(mPEG−SH) and heterobifunctional (HS−PEG−NH_2) poly(ethylene glycol) (PEGylation). Thereafter the terminal amino groups of the PEGylated particles (Au@mPEG−SH/HS−PEG−NH_2, **2**) are reacted with an amino-reactive, heterobifunctional, cross-linker (4-(*N*-maleimidomethyl)cyclohexane-1-carboxylic acid 3-sulfo-*N*-hydroxysuccinimide ester sodium salt or sulfo-SMCC) bearing a terminal maleimide functionality. In such a way, maleimide-functionalized gold nanoparticles (Au@mal, **3**) stable in biological media are obtained. The second step (Figure 1b) consists of the specific binding of the Au@mal nanoparticles (**3**) to a thiol-ended lipid (1,2-dipalmitoyl-*sn*-glycero-3-phosphothioethanol (sodium salt) or PTE−SH) (**4**) forming part of small fusogenic liposomes, via maleimide-sulfhydryl chemistry. Finally (Figure 1c), fusogenesis of the Au@mal-labeled liposomes (**5**) with the cellular membrane (of Jurkat cells in our case) (**6**) leads to the controlled delivery of the Au nanoparticles to the cellular membrane (**7**).

The initial PEGylation step has a 2-fold function. First, it increases the colloidal stability of the nanoparticles in the high ionic strength cellular medium, where the interparticle repulsion potential (in our case determined by the positive CTAB bilayer) can be fully screened leading to irreversible particle aggregation. Second, it makes them

DOI: 10.1021/nl101454a | *Nano Lett.* **2010,** *10,* 3006–3012

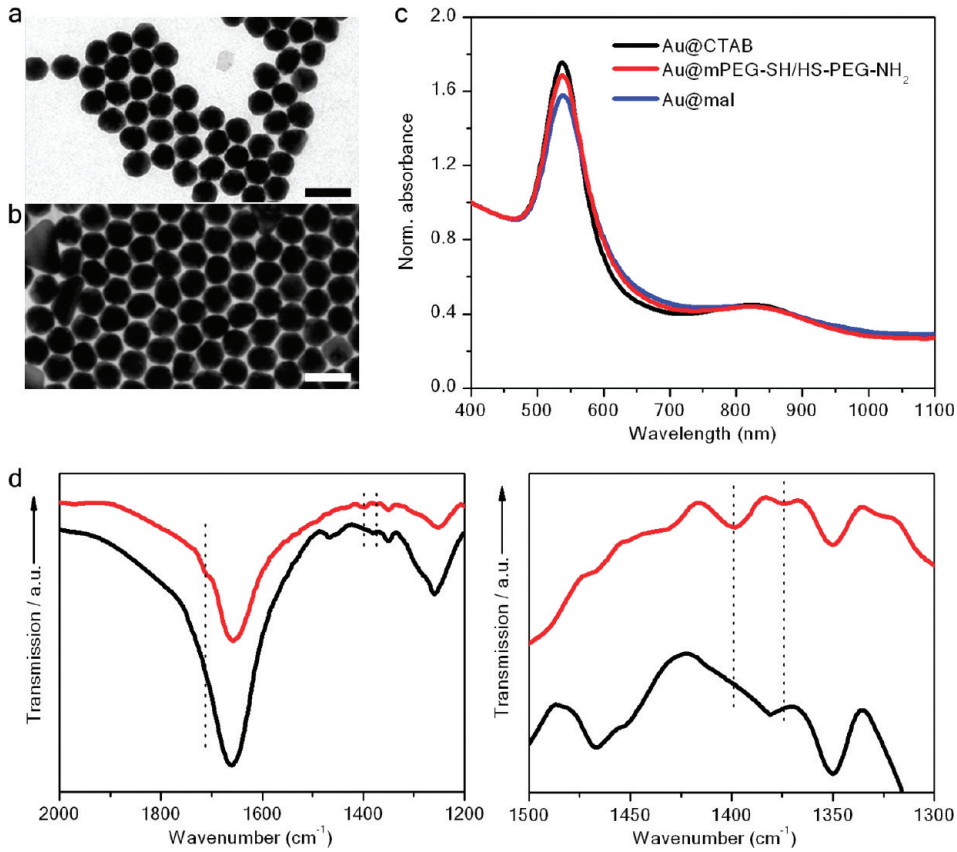

FIGURE 2. Representative transmission electron micrographs of the Au nanoparticles before (CTAB-capped) (a) and after (b) PEGylation/maleimide functionalization. Scale bars, 100 nm. (c) vis−NIR spectra of the Au@CTAB colloid after surface modification with mPEG−SH/HS−PEG−NH_2 and maleimide. The Au@CTAB nanoparticles are dispersed in water and Au@mPEG−SH/HS−PEG−NH_2 and Au@mal in PBS buffer (pH 7.6 and 6.9, respectively). The plasmon band is centered at 537 nm in all cases. The mode peaking at 820 nm is due to the nonspherical particles (~25%) present in the sample.[18] (d) FTIR spectra of Au@mPEG−SH/HS−PEG−NH_2 and Au@mal nanoparticles (black and red curves, respectively) in the range of 2000−1200 cm^{-1} (left panel). The right panel is an enlargement in the 1500−1300 cm^{-1} range.

biocompatible by reducing their cytotoxicity[21] and resistant against protein adsorption.[22] In addition, using a binary mixture of thiolated PEGs (prone to Au binding) bearing reactive and nonreactive terminal groups, serves as a platform for further surface modification,[22] where the number of reactive terminal groups (−NH_2 in our case) can be simply adjusted by modifying the ratio of both polymers.[23] As an additional advantage, the PEG-based coating allows for a direct control over the coating thickness by just changing the polymer molecular weight.

As a proof of principle, we have utilized CTAB-stabilized Au nanospheres (64 nm diameter, Figure 2a), synthesized as described elsewhere.[18] Surface grafting was performed with a mixture of mPEG−SH and HS−PEG−NH_2 (5000 Da in both cases, see Supporting Information) and resulted in a zeta potential (ζ) change from +40 to 0 mV, in agreement with previous reports.[21] No observable size or morphological changes occurred upon PEGylation. As further confirmed in the optical spectra shown in Figure 2c, the Au@mPEG−SH/HS−PEG−NH_2 nanoparticles remained stable after washing and final redispersion in PBS buffer (pH 7.6). No plasmon shift, just a slight decrease in extinction intensity was observed, suggesting that minor particle destabilization occurred.

In the next step the PEGylated particles were further functionalized using the available amino groups. For that purpose, we used an amino-reactive, water-soluble, and membrane impermeable heterobifunctional cross-linker (sulfo-SMCC, Figure 1a) bearing a terminal maleimide functionality. Sulfo-SMCC and analogous cross-linkers, containing succinimidyl ester and maleimide groups at respective ends, have been traditionally exploited for maleimide derivatization of amino-functionalized self-assembled monolayers on gold films.[24,25] Here, we have extended the usage of this cross-linker for maleimide-functionalization of our Au@mPEG−SH/HS−PEG−NH_2 nanoparticles. The reaction of the *N*-hydroxysulfosuccinimide ester of sulfo-SMCC is usually performed first in order to minimize hydrolysis, and under controlled pH conditions, to prevent reaction of the maleimide group with amines.[26,27] Typically, sulfo-SMCC is first coupled to molecules containing primary amines via amide bond formation buffered at pH 6.5−8.5 (Figure 1a), elimi-

DOI: 10.1021/nl101454a | *Nano Lett.* **2010,** *10,* 3006–3012

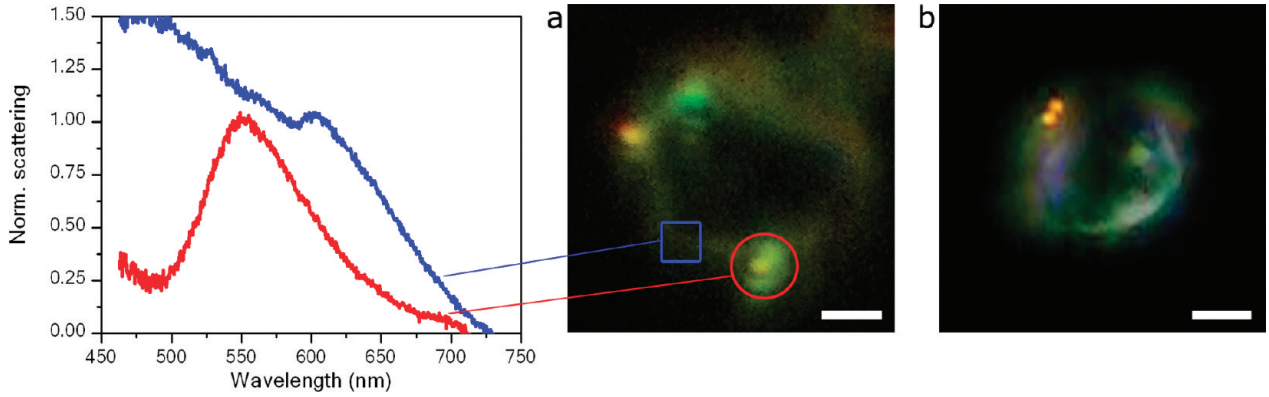

FIGURE 3. DFM images of a DPPC giant unilamellar vesicle (containing PTE−SH) after incubation with Au@mal (a) and Au@mPEG−SH/HS−PEG−NH_2 (b) nanospheres. Scale bars, 1 μm. The left panel shows the scattering spectra of the areas highlighted in (a): vesicle's lipid bilayer (square) and Au@mal nanoparticle bound to it (circle). For comparison, the spectra are normalized at 600 and 550 nm, respectively. The samples are suspended in a 0.13 M glucose solution for dark-field microspectroscopy characterization.

nating *N*-hydroxysulfosuccinimide as the leaving group. Thereafter it can be coupled to molecules containing free sulfhydryl groups via thioether linkage buffered at pH 6.5−7.0 (Figure 1b).[26] Compared to aromatic spacers, the cyclohexane bridge of sulfo-SMCC stabilizes the maleimide group prior to coupling.

The primary amines from the Au@mPEG−SH/HS−PEG−NH_2 nanoparticles were reacted with a 2-fold excess of sulfo-SMCC in PBS (pH 7.6) for 15 min. After washing the unreacted linker, the Au@mal nanoparticles were finally redispersed in PBS (pH 6.9). Maleimide derivatization was confirmed by Fourier transform infrared (FTIR) spectroscopy (Figure 2d). The FTIR spectrum of the Au@mal nanoparticles showed the characteristic asymmetric stretching mode of the imidyl group (O═C−N−C═O, 1712 cm^{-1}), the symmetric maleimide C−N−C stretching (1399 cm^{-1}) and the maleimide C−N stretching (1374 cm^{-1}), in agreement with the literature data.[25,28] The characteristic amide I or amide II bands of the newly formed amide linkage did not appear in the FTIR spectra, probably because the concentration is too low to be detected.[25] The zeta potential remained unchanged ($\zeta = 0$ mV) after maleimide functionalization. As shown in the TEM micrographs in Figure 2a and b, no observable changes occurred to the nanoparticles after PEGylation and maleimide derivatization. They remain stable, unaggregated, as further confirmed from the spectrum displayed in Figure 2c, where only a minor decrease in the plasmon intensity is observed.

In the next step we produced large liposomes (2−5 μm) consisting of SOPC (1-octadecanoyl-2-(9*Z*-octadecenoyl)-*sn*-glycero-3-phosphocholine), DOPE (1,2-di-(9-*Z*-octadecenoyl)-*sn*-glycero-3-phosphoethanolamine), and a small amount of a thiolated lipid (PTE−SH). We selected that lipid composition since it favors liposome fusogenesis with the plasma membrane of living cells,[29,30] as will be shown below. The role of PTE−SH is to provide a few thiol anchor points for the selective binding of the Au@mal nanoparticles, as sketched in Figure 1b. The ratio of maleimide groups on the nanoparticles to PTE−SH lipids in the liposomes was fixed to 1:5 and the reaction was performed in PBS (pH 6.9). The process effectively yielded Au@mal-labeled vesicles. However, the Au nanoparticles diffused fast on the liposomes since the latter are in fluid phase at room temperature. This issue hampered the realization of single particle spectroscopy (DFM) measurements on the Au nanoparticles. We overcomed this drawback by using large unilamellar (3−5 μm) DPPC (1,2-dipalmitoyl-*sn*-glycero-3-phosphocholine)/PTE−SH liposomes instead. The higher gel-to-fluid transition temperature of DPPC (41 °C) ensures low nanoparticle diffusion at room temperature, enabling DFM characterization. Figure 3a contains a representative DFM image from an Au@mal-labeled DPPC/PTE−SH vesicle. A relatively low particle loading (ca. 2−3 Au@mal nanoparticles/vesicle) was typically achieved under our experimental conditions. Nevertheless, by increasing the number of PTE−SH lipids in the vesicles and the concentration of Au@mal nanoparticles added, higher particle loadings could also be obtained. Importantly, most of the particles were bound to the vesicles in a single-particle fashion, effectively scattering green light under dark-field illumination and showing a clear localized surface plasmon resonance characteristic of individual Au nanospheres (see spectrum in Figure 3a). Compared to the spectrum of the ensemble in water (Figure 2c), the plasmon band of the single particles investigated was typically red-shifted (centered at 550 nm for the particular particle shown in Figure 3a). This is mainly ascribed to the refractive index increase from water ($n = 1.33$) to the aqueous glucose solution (0.13 M, $n = 1.34$,[31,32] see Supporting Information for details) where the Au@mal-labeled vesicles are suspended for DFM characterization, as well as to slight deviations from the sphericity of the particles measured.

Incubation of DPPC/PTE−SH vesicles with Au@mPEG−SH/HS−PEG−NH_2 nanoparticles under identical conditions typically yielded a lower particle loading, with many particles attaching as aggregates (Figure 3b), rather than as individual particles. The lack of preferential binding sites at the par-

DOI: 10.1021/nl101454a | *Nano Lett.* **2010,** *10,* 3006–3012

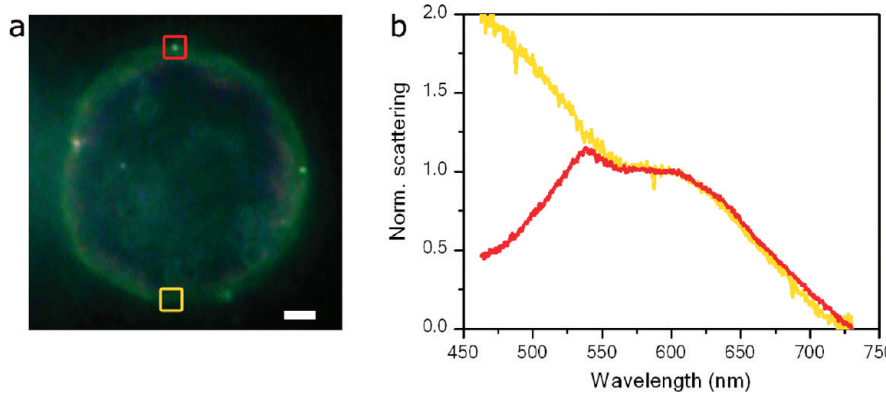

FIGURE 4. (a) Representative DFM image of a Jurkat cell after incubation with the Au@mal-labeled fusogenic liposomes. Scale bar, 2 μm. The Au@mal nanoparticles can be distinguished as green scattering spots on the cellular membrane. (b) Scattering spectra of the cell membrane and of a gold nanoparticle on it, yellow and red squares in (a), respectively. The spectra are normalized at 600 nm to facilitate comparison. The cells are suspended in PBS buffer (pH 6.9) during spectra collection.

ticles' surface toward PTE−SH results in unspecific adsorption. In contrast, the binding of the Au@mal nanoparticles is a chemically driven process directed by the high affinity of the maleimide terminal groups at the particles' surface toward the sulfhydryl-ended lipids at the vesicles. Note that the number of thiol groups per liposome was kept low so as to minimize particle aggregation and favor single particle binding upon maleimide−sulfhydryl reaction. An additional highlight on the versatility of our approach is that it could be possible to tune the experimental conditions so as to achieve monovalent PTE−SH binding, by simply minimizing the number of maleimide reactive groups at the Au nanoparticles surface (given by the number of $-NH_2$ functionalities introduced as HS−PEG−NH_2).

For the delivery of Au nanospheres to the plasma membrane of living cells, we have used small fusogenic vesicles[29,30] (120−620 nm, hydrodynamic diameter) consisting of SOPC and DOPE in a 3:1 ratio, and PTE−SH. The ratio of PTE−SH lipids in the liposomes to maleimide groups on the particles was set to 5:1 (see Supporting Information for experimental details), in order to minimize the number of unbound Au@mal nanoparticles after the maleimide−thiol reaction, since they could potentially bind to other thiolated molecules on the cellular membrane.

We selected a Jurkat (T-lymphocyte, nonadherent) cell line typically used to investigate transfection, as well as signaling events.[33,34] We incubated the Au@mal-labeled small liposomes with Jurkat cells so as to induce the fusogenesis (and lipid exchange) with the plasma membrane and thereby promote the incorporation of the Au@mal-tagged PTE−SH lipids (Figure 1c). As a result, single gold nanospheres (typically ca. three to five nanoparticles per cell) are effectively delivered to the cellular membrane and identified under the DFM as green scattering spots (Figure 4a). By following the approximation of Au@mal labeled fusogenic liposomes filled with fluorescein toward the cells in a DFM setup adjusted to detect scattering and fluorescence, we have observed that from ca. 10 events of contact liposome-cell ca. 2 lead to the successful delivery of gold nanoparticles to the cell membrane. Figure 4b contains representative scattering spectra of the plasma membrane and of an Au@mal nanoparticle bound to it. The membrane shows a rather featureless scattering spectrum characterized by a large scattering throughout the visible, particularly pronounced at the particle's plasmon resonance and lower wavelengths. While the scattering contribution from the membrane cannot be fully overcome in the background-corrected spectrum of the Au nanoparticle, its plasmon mode is clearly distinguishable at 538 nm.

In order to elucidate whether the as-delivered Au@mal nanoparticles are on the cell surface, we performed a control experiment based on the I_2/KI etching method recently reported by Xia and co-workers.[12] They have shown that Au nanoparticles attached to the cellular surface are readily oxidized upon addition of an I_2/KI mixture. This permits differentiating them easily from those being internalized into the cells. Prior to that control experiment, we first confirmed by vis−NIR spectroscopy that the Au@mal colloid in PBS is rapidly oxidized in the presence of I_2/KI (see Figure S1 in the Supporting Information). Our oxidation results for the Au@mal nanoparticles on the cell membrane are clearly illustrated in Figure 5. The scattering from the single gold nanoparticle shown dramatically decreases just a few seconds after the addition of the oxidizing mixture and fully vanishes after 24 s of reaction. These results confirm that our Au@mal nanoparticles are accessible to the I_2/KI mixture, and therefore we can conclude that they are effectively located on the cell membrane.

We further characterized the Au NP binding on the cell membrane with single nanoparticle tracking measurements. Figure 6 summarizes the characteristic diffusion behavior of many nanoparticles analyzed. The trajectories shown in panels b−e of Figure 6 are (x−y) projections of the particle diffusion on the cell surface, recorded at a constant focal plane in the DFM, as schematically sketched in Figure 6a. Visually, the Au@mal nanospheres bound to the PTE−SH

DOI: 10.1021/nl101454a | *Nano Lett.* **2010,** *10,* 3006–3012

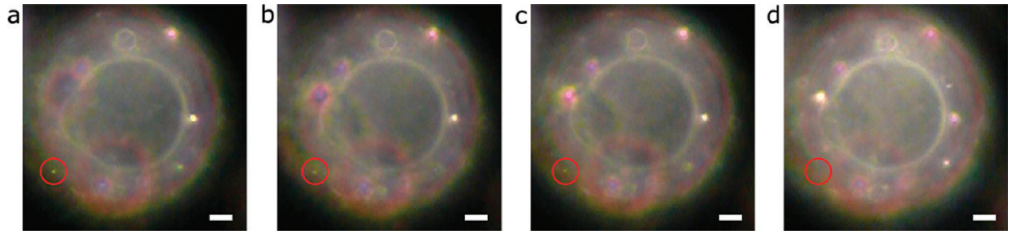

FIGURE 5. DFM images showing the oxidation of an Au@mal nanoparticle (highlighted) on the cell membrane of a Jurkat cell. The images are taken before (a) and 10 s (b), 16 s (c), and 24 s (d) after the addition of an I_2/KI aqueous solution. Scale bars, 2 μm.

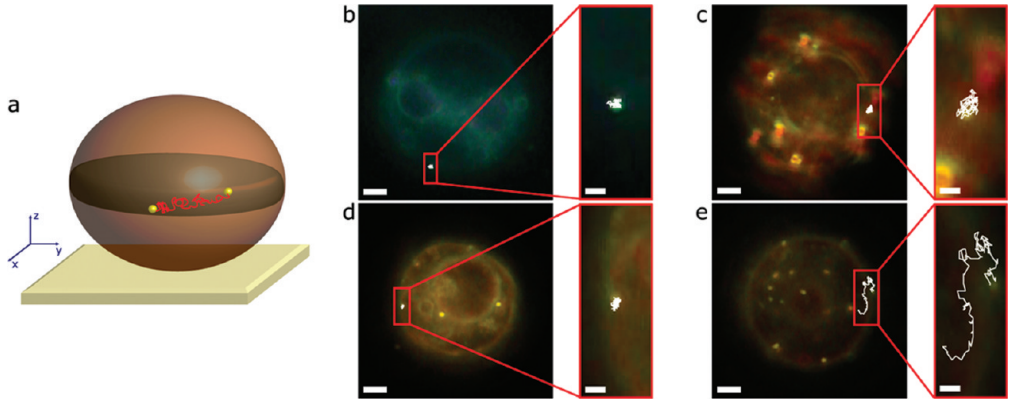

FIGURE 6. (a) Representative sketch (not to scale) depicting the diffusion of an Au nanoparticle on the cell surface. The particle remains at a constant focal plane during DFM observation and single particle tracking. (b–e) Optical DFM images showing representative two-dimensional (x–y projection) diffusion trajectories of individual Au nanoparticles on the surface of Jurkat cells. In each case Au-labeling was achieved via cell membrane fusogenesis with Au@mal-labeled liposomes (b) or after direct cell incubation with Au@mal (c, d) or Au@mPEG–SH (e) nanospheres. Scale bars, 2 μm. Right panels, enlargements (scale bars, 500 nm). A Semrock 532 nm single-edge dichroic beam splitter was used for DFM imaging (c–e).

lipids and incorporated on the cell membrane via fusogenesis appear to be immobile on the cell surface. Single nanoparticle tracking measurements revealed that all those nanospheres perform a rather slow (in the order of 0.0033 $\mu m^2\ s^{-1}$) and spatially limited diffusion over small cell membrane regions (Figure 6b). This behavior is consistent with reported constrained lipid diffusion in cellular membrane compartments.[35,36] For instance single particle tracking of 40 nm Au nanoparticles conjugated to DOPE lipids (via antigen–antibody recognition) has shown that the diffusion coefficient of DOPE in FRSK cells can be reduced ~10× (from 0.044 down to 0.0068 $\mu m^2\ s^{-1}$) after treatment with Jasplakinolide.[36] Jasplakinolide is a cyclic peptide that creates a coarser but stronger actin meshwork in the plasma membrane[37] and therefore sharply reduces lipid mobility. It is still unclear at this stage whether the immobilization of our Au@mal nanoparticles on the cell membrane could be due to an increase in the amount of picket proteins anchored along the membrane skeleton or to a preferential PTE–SH partitioning, among other factors.[35] Nevertheless our results support the mechanism according to which Au@mal-labeled liposomes merge with the cell membrane, lipid exchange occurs and the PTE–SH lipids to which the Au@mal nanoparticles are bound integrate within the membrane.

For reference experiments, we incubated the Jurkat cells directly (i.e., in the absence of the carrier fusogenic liposomes) with Au@mal and Au@mPEG–SH nanospheres. In both cases the yield of Au nanoparticle attachment to the cell surface was lower than that obtained when using the carrier Au@mal-labeled fusogenic liposomes. In contrast to the above results, the unspecifically attached Au@mal and Au@mPEG–SH nanoparticles presented different diffusion behaviors. Most of the Au@mal nanoparticles diffused faster on the cell membrane over larger distances (Figure 6c, D = 0.050 $\mu m^2\ s^{-1}$), while others performed a more limited, still fast, diffusion (Figure 6d, D = 0.106 $\mu m^2\ s^{-1}$). Upon direct incubation with the cells, the Au@mal nanoparticles can unspecifically react with any thiolated component of the plasma membrane (e.g., cysteine residues from enzymes or ion channels). Therefore, different diffusion lengths and times (Figure 6, panels c and d) occur depending on the Au@mal-tagged membrane entity. In this context, the nanoparticles' surface chemistry plays a major role on their nonspecific binding and diffusion on the cellular membrane.

In the case of the Au@mPEG–SH nanoparticles, the lack of functional reactive groups at the particles' surface resulted in weak particle adsorption at the cellular membrane, with a consequent quick diffusion (D = 0.0815 $\mu m^2\ s^{-1}$) over much larger distances (Figure 6e). In contrast to the above cases, most of the adsorbed Au@mPEG–SH nanoparticles detached from the cell surface.

DOI: 10.1021/nl101454a | *Nano Lett.* **2010,** *10,* 3006–3012

In conclusion, we have devised a general, versatile, and controlled strategy to bind individual gold nanoparticles to lipids in living cell membranes. Since our approach is based on lipid tagging, it allows for the preservation of the sensing and optothermal capabilities of the original Au colloid. We have shown that upon PEGylation and maleimide derivatization, CTAB-capped gold nanospheres can be conjugated to thiol-ended lipids in liposomes in a single-particle fashion. Fusogenesis of Au@mal-labeled fusogenic liposomes with the plasma membrane of living (Jurkat) cells leads to the controlled delivery of the gold nanoparticles to the cellular membrane. As a result of lipid binding, the gold nanoparticles perform a distinctively slow and spatially limited diffusion at the cell surface, consistent with reported constrained lipid diffusion in cellular membranes. Our method may be exploited as a general, versatile, and controlled way to routinely incorporate CTAB-capped colloids of varying composition, size, or shape onto cellular membranes and provides a powerful toolbox for the mapping, local sensing and (remote) manipulation of cell membrane processes.

Acknowledgment. Financial support by the DFG, through the Nanosystems Initiative Munich (NIM), and LMU*excellent* is gratefully acknowledged. We thank Alexander S. Urban for providing the script for single-particle tracking analysis; the group of Professor Hermann Gaub, for the cell culture facilities and excellent technical assistance; and Gerhard Sax and Jörg Schuster for assistance with the FTIR measurements. F.D.S. is a CONICET fellow.

Supporting Information Available. Experimental Section and time evolution of the vis-NIR extinction spectra of Au@mal nanoparticles upon oxidation with an I_2/KI mixture (Figure S1). This material is available free of charge via the Internet at http://pubs.acs.org.

REFERENCES AND NOTES

(1) Ranganathan, R. *Science* **2007**, *318*, 1253–1254.
(2) Pinaud, F.; King, D.; Moore, H.-P.; Weiss, S. *J. Am. Chem. Soc.* **2004**, *126*, 6115–6123.
(3) Gopakumar, G.; Christophe, D.; Paulina, I.; Michael, P.; Pierre-Yves, B.; Isabelle, G.; Davide, D.; Jacques, D.; Horst, V. *Angew. Chem., Int. Ed.* **2006**, *45*, 5478–5483.
(4) Mannix, R. J.; Kumar, S.; Cassiola, F.; Montoya-Zavala, M.; Feinstein, E.; Prentiss, M.; Ingber, D. E. *Nat. Nanotechnol.* **2008**, *3*, 36–40.
(5) Kotov, N. A.; Winter, J. O.; Clements, I. P.; Jan, E.; Timko, B. P.; Campidelli, S.; Pathak, S.; Mazzatenta, A.; Lieber, C. M.; Prato, M.; Bellamkonda, R. V.; Silva, G. A.; Kam, N. W. S.; Patolsky, F.; Ballerini, L. *Adv. Mater.* **2009**, *21*, 3970–4004.
(6) Sperling, R. A.; Gil, P. R.; Zhang, F.; Zanella, M.; Parak, W. J. *Chem. Soc. Rev.* **2008**, *37*, 1896–1908.
(7) Dahlin, A.; Zach, M.; Rindzevicius, T.; Kall, M.; Sutherland, D. S.; Hook, F. *J. Am. Chem. Soc.* **2005**, *127*, 5043–5048.
(8) Anker, J. N.; Hall, W. P.; Lyandres, O.; Shah, N. C.; Zhao, J.; Van Duyne, R. P. *Nat. Mater.* **2008**, *7*, 442–453.
(9) Álvarez-Puebla, R. A.; Liz-Marzán, L. M. *Small* **2010**, *6*, 604–610.
(10) Yao, C.; Rahmanzadeh, R.; Endl, E.; Zhang, Z.; Gerdes, J.; Huttmann, G. *J. Biomed. Opt.* **2005**, *10*, 064012–8.
(11) Urban, A. S.; Fedoruk, M.; Horton, M. R.; Rädler, J. O.; Stefani, F. D.; Feldmann, J. *Nano Lett.* **2009**, *9*, 2903–2908.
(12) Cho, E. C.; Xie, J.; Wurm, P. A.; Xia, Y. *Nano Lett.* **2009**, *9*, 1080–1084.
(13) Lee, C.-W.; Chen, M. J.; Cheng, J.-Y.; Wei, P.-K. *J. Biomed. Opt.* **2009**, *14*, 034016–6.
(14) Huang, X.; El-Sayed, I. H.; Qian, W.; El-Sayed, M. A. *J. Am. Chem. Soc.* **2006**, *128*, 2115–2120.
(15) Chen, J.; Wang, D.; Xi, J.; Au, L.; Siekkinen, A.; Warsen, A.; Li, Z.-Y.; Zhang, H.; Xia, Y.; Li, X. *Nano Lett.* **2007**, *7*, 1318–1322.
(16) Nikoobakht, B.; El-Sayed, M. A. *Chem. Mater.* **2003**, *15*, 1957–1962.
(17) Millstone, J. E.; Park, S.; Shuford, K. L.; Qin, L.; Schatz, G. C.; Mirkin, C. A. *J. Am. Chem. Soc.* **2005**, *127*, 5312–5313.
(18) Rodríguez-Fernández, J.; Pérez-Juste, J.; García de Abajo, F. J.; Liz-Marzán, L. M. *Langmuir* **2006**, *22*, 7007–7010.
(19) Grzelczak, M.; Pérez-Juste, J.; Mulvaney, P.; Liz-Marzán, L. M. *Chem. Soc. Rev.* **2008**, *37*, 1783–1791.
(20) Grzelczak, M.; Pérez-Juste, J.; Rodríguez-González, B.; Spasova, M.; Barsukov, I.; Farle, M.; Liz-Marzán, L. M. *Chem. Mater.* **2008**, *20*, 5399–5405.
(21) Niidome, T.; Yamagata, M.; Okamoto, Y.; Akiyama, Y.; Takahashi, H.; Kawano, T.; Katayama, Y.; Niidome, Y. *J. Controlled Release* **2006**, *114*, 343–347.
(22) Otsuka, H.; Nagasaki, Y.; Kataoka, K. *Adv. Drug Delivery Rev.* **2003**, *55*, 403–419.
(23) Mei, B. C.; Susumu, K.; Medintz, I. L.; Delehanty, J. B.; Mountziaris, T. J.; Mattoussi, H. *J. Mater. Chem.* **2008**, *18*, 4949–4958.
(24) Frey, B. L.; Corn, R. M. *Anal. Chem.* **1996**, *68*, 3187–3193.
(25) Xiao, S.-J.; Brunner, S.; Wieland, M. *J. Phys. Chem. B* **2004**, *108*, 16508–16517.
(26) Mattson, G.; Conklin, E.; Desai, S.; Nielander, G.; Savage, M. D.; Morgensen, S. *Mol. Biol. Rep.* **1993**, *17*, 167–183.
(27) Frey, B. L.; Jordan, C. E.; Kornguth, S.; Corn, R. M. *Anal. Chem.* **1995**, *67*, 4452–4457.
(28) Xiao, S.-J.; Wieland, M.; Brunner, S. *J. Colloid Interface Sci.* **2005**, *290*, 172–183.
(29) Miller, C. R.; Bondurant, B.; McLean, S. D.; McGovern, K. A.; O'Brien, D. F. *Biochemistry* **1998**, *37*, 12875–12883.
(30) Murcia, M. J.; Minner, D. E.; Mustata, G.-M.; Ritchie, K.; Naumann, C. A. *J. Am. Chem. Soc.* **2008**, *130*, 15054–15062.
(31) Kohl, M.; Cope, M.; Essenpreis, M.; Böcker, D. *Opt. Lett.* **1994**, *19*, 2170–2172.
(32) Lide, D. R. *CRC Handbook of Chemistry and Physics*, 85th ed.; CRC Press: FL, 2004.
(33) Bunnell, S. C.; Hong, D. I.; Kardon, J. R.; Yamazaki, T.; McGlade, C. J.; Barr, V. A.; Samelson, L. E. *J. Cell Biol.* **2002**, *158*, 1263–1275.
(34) Sumiyoshi, T.; Holt, N. G.; Hollis, R. P.; Ge, S.; Cannon, P. M.; Crooks, G. M.; Kohn, D. B. *Hum. Gene Ther.* **2009**, *20*, 1607.
(35) Kusumi, A.; Nakada, C.; Ritchie, K.; Murase, K.; Suzuki, K.; Murakoshi, H.; Kasai, R. S.; Kondo, J.; Fujiwara, T. *Annu. Rev. Biophys. Biomol. Struct.* **2005**, *34*, 351–378.
(36) Murase, K.; Fujiwara, T.; Umemura, Y.; Suzuki, K.; Iino, R.; Yamashita, H.; Saito, M.; Murakoshi, H.; Ritchie, K.; Kusumi, A. *Biophys. J.* **2004**, *86*, 4075–4093.
(37) Bubb, M. R.; Spector, I.; Beyer, B. B.; Fosen, K. M. *J. Biol. Chem.* **2000**, *275*, 5163–5170.

DOI: 10.1021/nl101454a | *Nano Lett.* **2010,** *10,* 3006–3012